Evidence for Large-Scale Eddy-Driven Gyres in the North Atlantic

M. Susan Lozier

Analysis of a recent climatological database for the North Atlantic has detailed an extensive large-scale recirculation system in the intermediate waters of the North Atlantic basin. The pressure fields that define this recirculation, coupled with the potential vorticity fields associated with the recirculating flow, provide observational evidence for basin-scale eddy-driven flow in the global ocean. The recirculations are intimately tied to the waters carried southward by the Deep Western Boundary Current and are therefore likely to affect the distribution of climatic anomalies in the North Atlantic.

The meridional thermohaline overturning cell in the Atlantic has been described as a conveyor belt, with surface waters transporting heat from the South Atlantic via swift, narrow boundary currents to the deep water formation sites in the northern North Atlantic. To complete the cycle, cold newly ventilated deep waters are exported from the high latitudes via the Deep Western Boundary Current, which follows the western boundary of the North and South Atlantic basins. Though attractive in its simplicity, this two-dimensional interpretation excludes recirculations in the horizontal plane.

Recirculations in the upper thermocline waters of the North Atlantic have been fairly well mapped compared with those in the deeper ocean, primarily because of differences in data resolution between the surface and deep ocean. However, a recent climatological database for the North Atlantic (*1*) has considerably improved the resolution of the intermediate and deep hydrographic property fields in the North Atlantic over previous global databases (*2*), chiefly by choosing smoothing scales specific to the relatively data-rich North Atlantic. One of the more intriguing features that has emerged from this hydrographic database is the detailed signature of extensive recirculations on surfaces of constant potential density anomaly (*3*), which are termed isopycnals, below the main thermocline (*1*) (Fig. 1). Isobars in the upper thermocline (Fig. 1A) trace the large-scale, anticyclonic subtropical gyre that is driven by the curl of the wind stress. The "bowl" formed by the isobars, with the depression located in the western portion of the gyre, is characteristic of all surfaces lying in the main thermocline. At the base of the thermocline (Fig. 1B), the isopycnals are relatively flat south of the Gulf Stream, which indicates the weakening of the direct wind forcing. The distinct lack of vertical shear in this area is consistent with the prior characterization (*4*) of this region as the weakly depth-dependent segment of the North Atlantic. Deeper in the water column (Fig. 1C), at ~2200 dbar, the isobars indicate a strong reappearance of recirculation with a pattern that is distinct from the recirculation in the upper thermocline (Fig. 1A). Instead of one broad recirculation that characterizes the wind-driven gyre in the upper thermocline waters, the pattern created by the isobars on this deep isopycnal defines several recirculation cells situated in the near vicinity of the Gulf Stream and North Atlantic Current. These individual recirculations, separated by low-pressure ridges, are linked to form a large-scale anticyclonic recirculation (*5*) that is in general agreement with a prior study based on quasi-synoptic data (*6*). As defined by the 2000- to 2200-dbar contours (Fig. 1C), the waters from the Gulf Stream are diverted into the North Atlantic Current, flow eastward over the Mid-Atlantic Ridge, recirculate anticyclonically southwest of Ireland (*7*), and flow westward back over the ridge (*8*). The flow continues along the western flank of the Mid-Atlantic Ridge, turning westward near 37°N to rejoin the Gulf Stream, thus forming a strong, extensive anticyclonic recirculation of the subtropical waters. These gyres are a persistent feature in the vertical, extending over ~1700 m of the water column. The horizontal extent of the gyres changes with depth; the maximum extent is on the surface shown in Fig. 1C. The recirculation shown by this pressure map (Fig. 1C) links previously observed local gyres (*9*) into a large-scale gyre that recirculates subtropical waters and entrains subpolar waters. In addition to the documented entrainment of Deep Western Boundary Current waters at these depths into the subtropical waters off of Cape Hatteras (*10*), this gyre system identifies a new pathway for subpolar waters to enter the subtropical gyre, namely from the southern branches of the North Atlantic Current on both sides of the Mid-Atlantic Ridge. A recent study on the spreading of Labrador Sea Water supports such a pathway (*11*).

The depth and structure of the intermediate recirculation in Fig. 1C weigh against wind forcing as the driving mechanism for this flow. Instead, the gyres could be eddy-driven (*12*) or created by pressure torques associated with bottom topography in a baroclinic ocean (*13*). Though the latter mechanism has been shown to produce recirculations at depth in non–eddy-resolving models (*14*), the horizontal and vertical structure of the gyres shown in Fig. 1C argues against such a choice as the primary driving mechanism (*15*). However, the alignment of the intermediate gyres with the western boundary current system and the gyres' maximal extent at mid-depth are consistent with eddy-driven flow. The forcing provided by eddy fluxes of potential vorticity, which are present as a result of the instability of the wind-driven flow, can produce closed geostrophic contours at depth. According to a theory formulated 15 years ago, potential vorticity is expected to be uniform within the regions of closed geostrophic contours, with the gradients of potential vorticity confined to the edges of the gyre (*16*). Numerical experiments with eddy-resolving quasi-geostrophic general circulation models have provided striking examples of deep eddy-driven gyres and their coincident pools of homogenous potential vorticity (*17*). When the North Atlantic potential vorticity field was previously examined for evidence of homogenization (*18*), a region of uniform potential vorticity was found in the upper thermocline. It remains ambiguous whether the observed uniformity is actually connected to the process of potential vorticity homogenization or whether it reflects the presence of a single water mass in the region, created by convective processes (*19*). These prior studies included only those waters above ~1100 m in the North Atlantic, leaving the depths below the main thermocline largely unexplored.

To study the potential vorticity signal associated with the noted recirculations, high-resolution fields of potential vorticity (*20*) were produced from the climatological database described in (*1*) (Fig. 2). In the upper thermocline (Fig. 2A), the potential vorticity contours trace the subtropical gyre pattern, but no homogenization is evident. The outcrop at the northern edge of the gyre provides ample ventilation to prevent homogenization. The field is marked by a sharp northward gradient across the Gulf Stream, which reflects the sharp decrease in layer thickness across that jet. A generally northward gradient of potential vorticity appears in the lower thermocline (Fig. 2B). This trend is interrupted at mid-latitudes by

Division of Earth and Ocean Sciences, Nicholas School of the Environment, Duke University, Box 90230, Durham, NC 27708–0230, USA.

a tongue of relatively high potential vorticity, supplied by the deep Mediterranean waters that spread westward to ~50°W (*21*). Unlike the upper thermocline, the potential vorticity gradient across the Gulf Stream is generally weaker than elsewhere on this isopycnal. As depth increases, the extent of this weakening increases until a pooling of waters with nearly uniform potential vorticity results. The pooling reaches its maximum spatial extent at a depth of approximately 2200 dbar (Fig. 2C), where the potential vorticity underneath the Gulf Stream, the North Atlantic Current, and their surroundings is virtually uniform. For even deeper surfaces, the pooling recedes and weakens, yielding a potential vorticity field that is generally dominated by planetary vorticity (*22*).

To show that the pool of nearly homogenous potential vorticity is generally coincident with the large-scale recirculation, an absolute velocity field (*23*) for the deep surface was superposed on its potential vorticity field for the area of interest (Fig. 3). The region of homogenized potential vorticity, shaded yellow, resides within the series of anticyclonic gyres west of the Mid-Atlantic Ridge (the recirculating gyres of the Sargasso Sea and the Newfoundland basin), lending credence to the supposition that the homogenization of potential vorticity is a consequence of the recirculation.

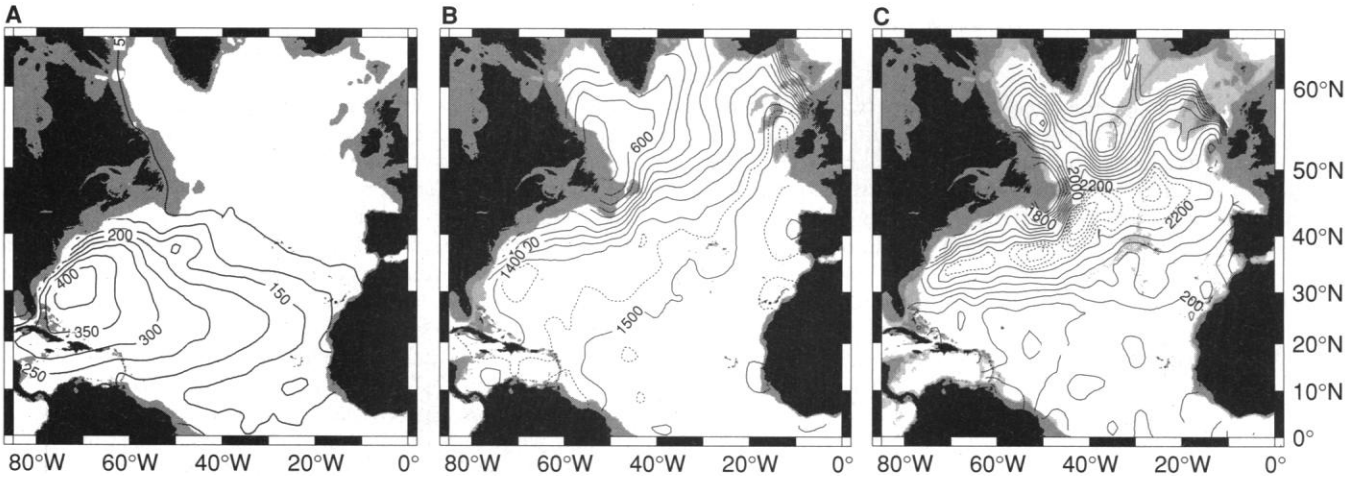

Fig. 1. Pressure in decibars on three selected isopycnals, $\sigma_0 = 26.50$ (**A**), $\sigma_{1.5} = 34.60$ (**B**), and $\sigma_2 = 36.95$ (**C**), which represent upper thermocline waters, lower thermocline waters, and deep waters of the subtropical North Atlantic, respectively. Because the horizontal pressure gradient on an isopycnal is essentially equivalent to the slope of an isopycnal, a pressure map yields the approximate direction of the vertical shear. The horizontal pressure gradient imposed by sea surface topography is unknown; therefore the pressure gradient deduced from the density field alone (that is, from the hydrography) yields information on the relative flow field only. If one assumes that the velocity field goes to zero at a location in the water column (a level-of-no-motion assumption), the isobars approximate absolute flow lines. A deep level of no motion for the subtropical circulation, including the Gulf Stream, its recirculations, and its extension into the North Atlantic Current, is used for the interpretation of these pressure maps; thus high pressures are to the right of the flow, looking downstream. For $\sigma_0 = 26.50$ (A), the pressure is contoured at 50 dbar. This surface outcrops in winter between the 50- and 100-dbar contour. For $\sigma_{1.5} = 34.60$ (B), the pressure is contoured at 100 dbar (solid lines) except for the 1450- and 1550-dbar contours (dashed lines). For $\sigma_2 = 36.95$ (C), the pressure is contoured at 50 dbar (solid lines); the recirculations are detailed with 25 dbar contours from 2200 to 2325 dbar (dashed lines). Bathymetry <500 m is shaded dark gray for all surfaces, bathymetry <1000 m is shaded medium gray in (B) and (C), and bathymetry <2000 m is shaded light gray in (C).

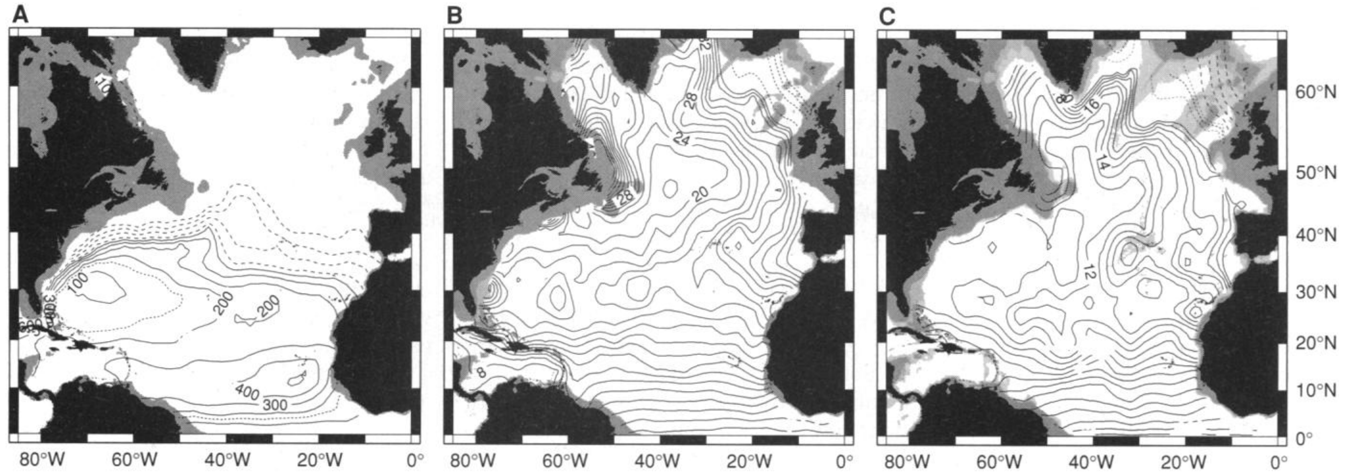

Fig. 2. Potential vorticity on the same isopycnals as in Fig. 1. For $\sigma_0 = 26.50$ (**A**), the contour intervals are 100 (solid lines) and 200 (long-dashed lines) $\times 10^{-12}$ m^{-1} s^{-1} bar. The 150×10^{-12} m^{-1} s^{-1} contour is designated with a short-dashed line. For $\sigma_{1.5} = 34.60$ (**B**), the contour intervals are 2 (solid lines) and 50 (dashed lines) dbar. For $\sigma_2 = 36.95$ (**C**), the contour intervals are 1 (solid lines), 10 (short-dashed lines), and 100 (long-dashed lines) $\times 10^{-12}$ m^{-1} s^{-1}. Bathymetry is as in Fig. 1. The deep potential vorticity field (C) preserves its uniformity even when contoured at the level of the computed standard errors (0.2 to 0.4×10^{-12} m^{-1} s^{-1} in the western North Atlantic).

Actually, the existence of the coincident, homogeneous, potential vorticity pool is itself evidence for the existence of the recirculation. The relatively low value of potential vorticity within the pool reflects the tendency of western-intensified anticyclonic flow to preferentially advect waters from the southern rim of the gyre into the gyre interior (*24*). Finally, the southern rim of the potential vorticity pool in the western North Atlantic coincides with a region where the necessary conditions for flow instability are met, thus suggesting a source for mesoscale eddies in the flow field (*25*).

In contrast to the gyres west of the Mid-Atlantic Ridge, the anticyclonic gyre east of the ridge is characterized by a sizable east-west gradient of potential vorticity (Fig. 2C). There is no difference in the standard errors for the pressure fields east and west of the ridge, and the standard errors for potential vorticity are only slightly larger ($\sim 0.6 \times 10^{-12}$ m^{-1} s^{-1}) east of the ridge than west of the ridge (~ 0.2 to 0.4×10^{-12} m^{-1} s^{-1}). Thus, there is little reason to suspect that the fields east of the ridge are any less representative than those to the west. Rather, it is hypothesized that the conditions required for potential vorticity homogenization are not met in this locale. It is central to the theory of potential vorticity homogenization that there are no local sources of potential vorticity in the locale; such a source would inhibit homogenization by essentially resetting the value of potential vorticity as the fluid circulated about the gyre. On the deep surface (Fig. 2C), the highest value of potential vorticity occurs in the northeast corner of the basin, where the isopycnal rises rapidly to the upper water column, which is strongly stratified. Because these high-potential-vorticity waters contrast sharply with the low-potential-vorticity waters recirculating in the gyre, it is suggested that the concomitant strong diffusive fluxes would prevent homogenization of potential vorticity in this region (*26*).

On the basis of the work presented here, it is hypothesized that the signature of gyres in the intermediate North Atlantic waters is an expression of eddy-driven flow. This hypothesis is based on the following reasons. First, the gyres appear at intermediate depths isolated from the direct wind or buoyancy forcing of the upper waters and the strong topographic forcing of the abyssal waters. Second, the gyres are strongly linked to the eddy-rich Gulf Stream and North Atlantic Current. Using observations at two mooring sites in the Gulf Stream, Hogg showed that eddy fluxes are strong enough to force significant recirculation gyres in the deep ocean (*27*). Third, potential vorticity is homogeneous within the gyres, with the extent of the homogeneous pool of potential vorticity maximized at the depth at which the recirculation is strongest, as measured by the local gradient of the pressure field. An examination of the pressure fields and potential vorticity fields shows that as the recirculation weakens, the pool recedes, which strongly suggests that these features are dynamically linked.

The particular eddy mechanism driving this flow cannot easily be deduced from the climatological fields. One theory of eddy-driven flow predicts that baroclinic eddies, acting on the large-scale Sverdrup flow, would create closed geostrophic contours at depth (*28*). A second theory attributes the production of closed streamlines in the ocean interior to the eddies transported by a western boundary current, which is appended to the recirculating gyres (*29*). The vertical structure of the gyres and their proximity to the Gulf Stream and North Atlantic Current favors the second theory, but more investigation is needed before either theory of eddy-driven flow can be validated by these observations.

The large-scale recirculation at intermediate depths in the North Atlantic affects the propagation of climatic anomalies from the convective sites in the northern North Atlantic in two important ways. First, it provides a pathway other than the Deep Western Boundary Current for newly ventilated deep water to enter the subtropical gyre. Second, recirculations can modulate the signal and increase the residence time for properties carried equatorward from the convective sites. Evidence for such an impact comes from observations of tracers in the subtropical gyre and the adjoining Deep Western Boundary Current (*30*). In particular, a minimum in chlorofluorocarbon concentrations (a tracer of newly ventilated waters) coincides with the depth range at which these intermediate recirculations exist. Although the intermittency of deep water formation in this depth range is also an important factor in the determination of this signal, this coincidence suggests that these recirculations may contribute to this minimum through the dilution of the tracer signal. Finally, the existence of these recirculations may have to be taken into account in paleoceanographic reconstructions of meridional circulation in the North Atlantic.

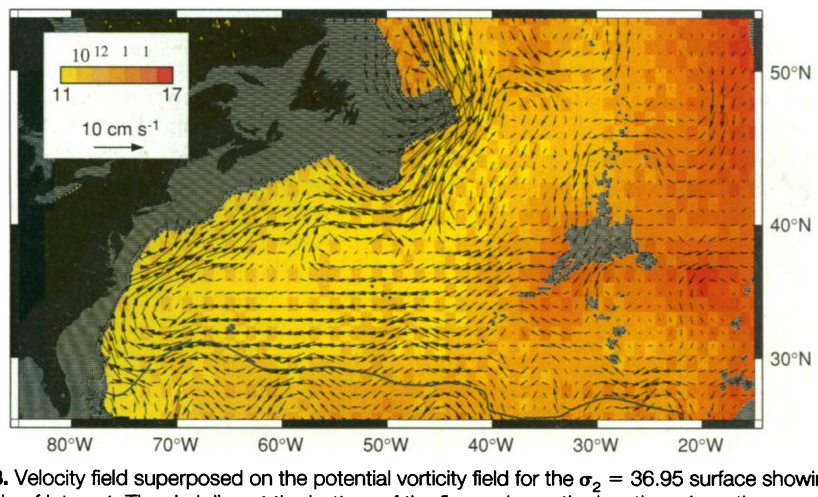

Fig. 3. Velocity field superposed on the potential vorticity field for the $\sigma_2 = 36.95$ surface showing the domain of interest. The dark line at the bottom of the figure shows the location where the upper layer potential vorticity gradient changes sign (Fig. 2A). Because this flow field was calculated with a deep level of no motion for the entire region, the Deep Western Boundary Current (for which a shallow level of no motion is appropriate) is reversed. Unless one makes some arbitrary choice as to where the level of no motion should change, the two juxtaposed flows (the deep Gulf Stream and the Deep Western Boundary Current) cannot be easily delineated. Bathymetry <1000 m is shaded dark gray and bathymetry <2000 m is shaded light gray.

REFERENCES AND NOTES

1. M. S. Lozier, W. B. Owens, R. G. Curry, *Prog. Oceanogr.* **36**, 1 (1995).
2. S. Levitus, *NOAA Prof. Pap. 13* (Government Printing Office, Washington, DC, 1982); S. Levitus and T. P. Boyer, *World Ocean Atlas 1994*, vol. 4, *Temperature*, NOAA Atlas NESDIS 4 (National Oceanic and Atmospheric Administration, Washington, DC, 1994).
3. Potential density is the density of seawater calculated with a reference pressure, rather than in situ pressure, in order to remove compressibility effects. The potential density anomaly (σ_n, in kilograms per cubic meter) is defined as potential density − 1000 kg m^{-3}. The reference pressure divided by 1000 dbar is denoted by *n*. The depth of the potential density anomaly surface is approximated by its pressure, because 1 dbar ~ 1 m.
4. W. J. Schmitz, *J. Mar. Res.* **38**, 111 (1980).
5. Because the detailed signature of the recirculation was created by isobars contoured between 25 and 50 dbar, it is important to note that the standard errors for the pressure field on this surface are ~10 to 20 dbar for the western North Atlantic.
6. An earlier analysis of a collection of historical hydrographic lines [J. L. Reid, *Prog. Oceanogr.* **33**, 1

(1994)] showed a large-scale anticyclonic gyre in the general vicinity of the gyre shown in Fig. 1C. However, Reid's gyre and the one depicted in Fig. 1C have substantial differences in their vertical structure and horizontal substructure.
7. Southward flow of North Atlantic Deep Water on the eastern side of the Mid-Atlantic Ridge is supported by P. M. Saunders [*J. Mar. Res.* **40**, 641 (1982)], S. Gana and C. Provost [*J. Mar. Syst.* **4**, 67 (1993)], and J. Paillet and H. Mercier (*Deep-Sea Res., Part I*, in press).
8. Topographic sill depths of ~1000 m are a barrier for flow of this density into the Nordic Seas.
9. L. V. Worthington, *Johns Hopkins Oceanogr. Stud.* **6**, (1976); R. A. Clarke, H. W. Hill, R. F. Reininger, B. A. Warren, *J. Phys. Oceanogr.* **10**, 25 (1980); M. S. McCartney, *Prog. Oceanogr.* **29**, 283 (1992); W. J. Schmitz and M. S. McCartney, *Rev. Geophys.* **31**, 29 (1993).
10. R. S. Pickart and W. M. Smethie, *J. Phys. Oceanogr.* **23**, 2602 (1993).
11. J. Paillet, M. Arhan, M. S. McCartney, in preparation.
12. P. B. Rhines and W. R. Holland, *Dyn. Atmos. Oceans* **3**, 289 (1979).
13. W. R. Holland, *Geophys. Fluid Dyn.* **4**, 187 (1973).
14. R. Gerdes and C. Köberle, *J. Phys. Oceanogr.* **25**, 2624 (1995).
15. These gyres at intermediate depths are distinct from the smaller scale gyres at abyssal depths that are more clearly associated with the basin topography.
16. P. B. Rhines and W. R. Young, *J. Fluid Mech.* **122**, 347 (1982).
17. W. R. Holland and P. B. Rhines, *J. Phys. Oceanogr.* **10**, 1010 (1980).
18. S. McDowell, P. Rhines, T. Keffer, *ibid.* **12**, 1417 (1982); T. Keffer, *ibid.* **15**, 509 (1985); J. L. Sarmiento, C. G. H. Rooth, W. Roether, *J. Geophys. Res.* **87**, 8047 (1982).
19. J. Pedlosky, *Ocean Circulation Theory* (Springer-Verlag, New York, 1996).
20. Potential vorticity is calculated as $f\,{}^1/\sigma_0 \times \partial\sigma_n/\partial z$, where f is the planetary vorticity, z is the vertical coordinate, and σ_0 is a constant potential density. The vertical derivative is computed locally over a nominal depth of 100 m. In an effort to approximate neutral surfaces [T. J. McDougall, *J. Phys. Oceanogr.* **17**, 1950 (1987)], potential vorticity was also calculated as f/h, where h is the distance between two locally referenced isopycnals. The differences in the two methods were insignificant to the results of this study; that is, the region and extent of homogenization were the same with either calculation.
21. M. S. McCartney and L. D. Talley, *ibid.* **12**, 1169 (1982).
22. J. O'Dwyer and R. G. Williams (*J. Phys. Oceanogr.*, in press) report, from an analysis of the Levitus data set, possible regions of homogenization at abyssal depths in the western North Atlantic.
23. An absolute flow field was calculated for $\sigma_2 = 36.95$ by differentiation of a modified [H.-M. Zhang and N. G. Hogg, *J. Mar. Res.* **50**, 385 (1992)] Montgomery stream-function field [R. B. Montgomery, *Bull. Am. Meteorol. Soc.* **18**, 210 (1937)] with $\sigma_3 = 41.45$ (at ~3000 m) as the level of no motion.
24. D. L. Musgrave, *J. Geophys. Res.* **90**, 7037 (1985).
25. Surfaces shallower than $\sigma_2 = 36.95$ show counter-rotating gyres separated by this instability region in the western North Atlantic, which suggests the importance of eddy flux divergence in the forcing of the gyres.
26. J. Pedlosky, *J. Phys. Oceanogr.* **13**, 2121 (1983).
27. N. Hogg, *Deep-Sea Res. Part A* **30**, 945 (1983).
28. P. B. Rhines and W. R. Young, *J. Mar. Res.* **40**, 559 (1982).
29. P. Cessi, G. Ierley, W. Young, *J. Phys. Oceanogr.* **17**, 1640 (1987); P. Cessi, *ibid.* **18**, 662 (1988).
30. W. J. Jenkins and P. B. Rhines, *Nature* **286**, 877 (1980); R. S. Pickart, *Deep-Sea Res. Part A* **39**, 1553 (1992); W. M. Smethie, *Prog. Oceanogr.* **31**, 51 (1993).
31. I thank J. Pedlosky for his aid in the interpretation of these fields and P. Rhines for his comments on the manuscript. Support from NSF (grant OCE-9629489) is gratefully acknowledged.

20 February 1997; accepted 22 May 1997

Maximum and Minimum Temperature Trends for the Globe

David R. Easterling,* Briony Horton, Philip D. Jones, Thomas C. Peterson, Thomas R. Karl, David E. Parker, M. James Salinger, Vyacheslav Razuvayev, Neil Plummer, Paul Jamason, Christopher K. Folland

Analysis of the global mean surface air temperature has shown that its increase is due, at least in part, to differential changes in daily maximum and minimum temperatures, resulting in a narrowing of the diurnal temperature range (DTR). The analysis, using station metadata and improved areal coverage for much of the Southern Hemisphere landmass, indicates that the DTR is continuing to decrease in most parts of the world, that urban effects on globally and hemispherically averaged time series are negligible, and that circulation variations in parts of the Northern Hemisphere appear to be related to the DTR. Atmospheric aerosol loading in the Southern Hemisphere is much less than that in the Northern Hemisphere, suggesting that there are likely a number of factors, such as increases in cloudiness, contributing to the decreases in DTR.

The global mean surface air temperature has risen about 0.5°C during the 20th century (*1*). Analysis has shown that this rise has resulted, in part, from the daily minimum temperature increasing at a faster rate or decreasing at a slower rate than the daily maximum, resulting in a decrease in the DTR for many parts of the world (*2, 3*). Decreases in the DTR were first identified in the United States, where large-area trends show that maximum temperatures have remained constant or have increased only slightly, whereas minimum temperatures have increased at a faster rate (*4*). Similar changes have been found for other parts of the world as data have become available, allowing more global analyses (*2, 3*). However, in some areas the pattern has been different: In parts of New Zealand (*5*) and alpine regions of central Europe (*6*), maximum and minimum temperature have increased at similar rates, and in India, the DTR has increased as a result of a decrease in the minimum temperature (*7*). To evaluate these varying results, we conducted an expanded analysis on global and regional scales.

Local effects such as urban growth, irrigation, desertification, and variations in local land use can all affect the DTR (*3*); in particular, urbanized areas often show a narrower DTR than nearby rural areas (*8*). Large-scale climatic effects on the DTR include increases in cloud cover, surface evaporative cooling from precipitation, greenhouse gases, and tropospheric aerosols (*9, 10*). Recent studies have demonstrated a strong relation between trends of the DTR and decreases in pan evaporation over the former Soviet Union and the United States (*11*), suggesting that the DTR decrease in these areas is influenced by increases of cloud amount and reduced insolation (*1*). Furthermore, recent modeling studies have suggested that the decrease in the DTR may be a result of a combination of direct absorption of infrared portions of incoming solar radiation, aerosols, and water-vapor feedbacks, including surface evaporative effects (*12*).

We analyzed monthly averaged maximum and minimum temperatures and the DTR at 5400 observing stations around the world. Each time series from each station was subjected independently to homogeneity analyses and adjustments according to recently developed techniques (*13*). In general, these homogeneity adjustments have little effect on large-area averages (global or hemispheric), but they can have a noticeable effect on smaller regions (*14*), particularly when comparing trends at individual or adjacent grid boxes.

Our data covers 54% of the total global land area, 17% more than in previous studies (*3*). Most of the increases are in the Southern Hemisphere, with the addition of data for South America, New Zealand, all of Australia, a number of Pacific islands, and Indonesia. Data were also in-

D. R. Easterling, T. C. Peterson, T. R. Karl, National Climatic Data Center, Asheville, NC 28801, USA.
B. Horton, D. E. Parker, C. K. Folland, Hadley Center, Meteorological Office, Bracknell, Berkshire, UK.
P. D. Jones, Climatic Research Unit, University of East Anglia, Norwich, UK.
M. J. Salinger, National Institute of Water and Atmospheric Research, Auckland, New Zealand.
V. Razuvayev, All-Russia Research Institute of Hydrometeorological Information, Obninsk, Russia.
N. Plummer, National Climate Center, Bureau of Meteorology, Melbourne, Australia.
P. Jamason, DynTel Inc., National Climatic Data Center, Asheville, NC 28801, USA.

*To whom correspondence should be addressed: E-mail: deasterl@ncdc.noaa.gov